






## Hydrostatic pressure induces transformations in the organic matter and microbial community composition of marine snow particles

Peter Stief <sup>1</sup>✉, Clemens Schauburger <sup>1</sup>, Kevin W. Becker <sup>2</sup>, Marcus Elvert<sup>3</sup>, John Paul Balmonte<sup>1</sup>, Belén Franco-Cisterna<sup>1</sup>, Mathias Middelboe <sup>1,4</sup> & Ronnie N. Glud <sup>1,5,6</sup>

In the hadal zone of the ocean (6–11 km), the characteristics of sinking marine snow particles and their attached microbial communities remain elusive, despite their potential importance for benthic life thriving at extreme pressures (60–110 MPa). Here, we used simulation experiments to explore how increasing pressure levels modify the microbial degradation, organic matter composition, and microbiome of sinking diatom aggregates. Individual aggregates were incubated in rotating tanks in which pressure was incrementally increased to simulate a descent from surface to hadal depth within 20 days. Incubations at atmospheric pressure served as controls. With increasing pressure, microbial respiration and diatom degradation decreased gradually and ceased completely at 60 MPa. Dissolved organic carbon leaked substantially from the aggregates at  $\geq 40$  MPa, while diatom lipid and pigment contents decreased moderately. Bacterial abundance remained stable at  $>40$  MPa, but bacterial community composition changed significantly at 60–100 MPa. Thus, pressure exposure reduces microbial degradation and transforms both organic matter composition and microbiomes of sinking particles, which may seed hadal sediments with relatively fresh particulate organic matter and putative pressure-tolerant microbes.

<sup>1</sup>Department of Biology, HADAL & Nordcee, University of Southern Denmark, Odense, Denmark. <sup>2</sup>GEOMAR Helmholtz Center for Ocean Research, Kiel, Germany. <sup>3</sup>MARUM - Center for Marine Environmental Sciences and Faculty of Geosciences, University of Bremen, Bremen, Germany. <sup>4</sup>Marine Biological Section, Department of Biology, University of Copenhagen, Helsingør, Denmark. <sup>5</sup>Danish Institute for Advanced Study, University of Southern Denmark, Odense, Denmark. <sup>6</sup>Tokyo University of Marine Science and Technology, Tokyo, Japan. ✉email: [peterstief@biology.sdu.dk](mailto:peterstief@biology.sdu.dk)

Photosynthetic biomass production by phytoplankton is a major source of organic particles in the euphotic zone of the ocean. These particles sink to depth as dense aggregations of microalgal and prokaryotic cells or repackaged into zooplankton fecal pellets, collectively referred to as marine snow<sup>1,2</sup>. Gravitational sinking of particles drives the biological carbon pump in the ocean and supplies deep-sea biota with organic substrates<sup>3,4</sup>. In the epi- and mesopelagic zone, particles may sink through steep gradients of light, temperature, and inorganic nutrients and encounter abundant zooplankton. Particle degradation by heterotrophic bacteria as well as particle grazing by zooplankton are intense in these zones<sup>5–8</sup>. The vertical carbon flux is strongly attenuated by these processes, which reduces the efficiency of the biological carbon pump to sequester atmospheric carbon dioxide in the deep ocean<sup>9</sup>.

The degradation of sinking particles has mainly been studied in the epi- and mesopelagic zone (i.e., at <1000 m water depth). Particle transformations in the deep ocean (i.e., at >1000 m water depth) have received less attention<sup>10</sup>. In the deep ocean, the vertical carbon flux is low and nearly constant with depth, which implies that here particle degradation is rather limited<sup>9</sup>. Reduced particle degradation may be partially due to low temperatures prevailing in the deep ocean<sup>11,12</sup>. Other studies have identified hydrostatic pressure as an environmental factor reducing particle-associated respiration activity, a proxy for microbial particle degradation through oxidative carbon mineralization<sup>13,14</sup>. However, previous pressure incubations rarely exceeded 40 MPa (corresponding to 4 km water depth) or involved only a single shift between atmospheric and one high-pressure level<sup>13–16</sup>. Consequently, it remains unresolved to what extent marine snow particles are degraded and otherwise transformed during the descent from the surface ocean into the hadal realm where they experience pressure levels of 60–110 MPa.

High hydrostatic pressure levels impede biochemical processes in microorganisms adapted to atmospheric pressure levels<sup>17–20</sup>. Amongst others, high-pressure levels lower membrane fluidity, promote protein dissociation and unfolding, stabilize hydrogen bonds in DNA, and cause ribosome dissociation. Consequently, cellular processes related to energy conservation, DNA replication, and RNA translation may become dysfunctional, which can prohibit microbial cells from growing and dividing. At the level of microbial communities, pressure can thus be a selective factor potentially influencing community composition. Surface-derived marine microbial communities exposed to increasing pressure levels show significant compositional changes<sup>13,21,22</sup>. However, none of these studies tested the effect of the pressure levels prevailing in the hadal realm (60–110 MPa) on the composition of particle-attached microbial communities. During their descent through the deep ocean, particles might also be colonized by residential piezotolerant or piezophilic bacteria. However, the colonization of sinking particles by free-living bacteria has repeatedly been shown to occur mainly during particle formation in the epipelagic zone<sup>4</sup> and seems quantitatively not significant below the epipelagic zone<sup>23</sup>. The extent to which successional dynamics of particle-attached communities are altered at pressure levels characteristic of the bathypelagic zone and below is generally little understood.

Using model diatom aggregates, we simulated the complete pressure history of particles sinking from the ocean surface into a hadal trench. As most hadal trenches are located along continental margins and thus relatively close to land, many of them are overlain by productive waters (e.g., Japan trench, South Sandwich trench, Atacama trench)<sup>24–26</sup>. Coastal upwelling and dust inputs from the nearby land favor seasonal blooms of pelagic diatoms<sup>27,28</sup>. Ballasted by their silica shell, diatoms display particularly high sinking rates when aggregated to marine snow

particles<sup>6,29</sup>. Diatom aggregates are thus more likely to sink all the way down to hadal depth than aggregates formed by less abundant and less ballasted phytoplankton groups.

Individual diatom aggregates were kept sinking in rotating pressure tanks in which pressure was incrementally increased from 0.1 to 100 MPa within 20 days (Fig. 1). This pressure scheme corresponds to the relatively fast sinking velocity of model diatom aggregates of 500 m d<sup>-1</sup> and may allow successions of the microbial community associated with diatom aggregates in response to the gradual pressure increase<sup>11,14</sup>. As a negative control, diatom aggregates were kept sinking in rotating control tanks in which pressure was left at atmospheric level (0.1 MPa) for 20 days. Microbial particle degradation was followed in real-time through continuous respiration measurements inside the incubation tanks. The transformation of organic constituents of the aggregates (i.e., dissolved organic carbon, diatom lipids and photopigments) was followed in samples retrieved in steps of 20 MPa in pressure tanks operated in parallel. Using the same sampling scheme, succession of prokaryotic communities was followed through 16S rRNA gene amplicon sequencing. This study revealed that high pressure levels inhibit microbial degradation of sinking diatom aggregates, but stimulate substantial leakage of dissolved organic carbon from the aggregates. Additionally, it was shown that the microbiomes of the aggregates are thoroughly re-shaped by high-pressure levels.

## Results

### Aggregate degradation

**Respiration activity.** As a proxy for microbial aggregate degradation through oxidative carbon mineralization, oxygen consumption by 14 individual diatom aggregates was continuously measured as a decrease in oxygen concentration at either atmospheric pressure (control treatment) or increasing pressure (pressure treatment) (Fig. 2a–c). In the control treatment, oxygen consumption remained high during the first half of the incubation period and then decreased moderately during the second half (Fig. 2d–f). In the pressure treatment, however, oxygen consumption first decreased gradually (0.1–40 MPa) and then ceased completely (60–100 MPa) (Fig. 2d–f).

**Exoenzyme activities.** The activities of five exoenzymes associated with the diatom aggregates were measured to quantify hydrolysis of polymeric organic compounds as the first and potentially rate-limiting step of carbon mineralization. In most cases, mean hydrolysis rates were not statistically different between the control and pressure treatment (Student's *t*-test:  $p > 0.05$ ) (Supplementary Fig. 1). However, mean rates of the protein-degrading enzyme leucine aminopeptidase were consistently higher in the pressure treatment (Supplementary Fig. 1a). In contrast, mean rates of the carbohydrate-degrading enzymes  $\beta$ -glucosidase, laminarinase, and pullulanase were mostly lower in the pressure treatment (Supplementary Fig. 1b–d). Notably, pullulanase and  $\beta$ -glucosidase activities were significantly reduced at pressure levels of 20 MPa and 60 MPa, respectively (Student's *t*-test:  $t = 2.80$ ,  $df = 6$ ,  $p = 0.031$  and  $t = 3.29$ ,  $df = 6$ ,  $p = 0.017$ ). No activity was detected for chondroitin sulfatase.

**Dissolved organic carbon (DOC) leakage.** In the control treatment, net uptake and/or consumption of ambient DOC was observed over time (Fig. 3a–c). In the pressure treatment, however, striking increases in ambient DOC concentrations occurred at 40–60 MPa (corresponding to simulated sinking depths of 4–6 km), suggesting pressure-induced DOC leakage from aggregates (Fig. 3a–c).

Pressure-induced DOC leakage from the aggregates was most likely due to *Skeletonema marinoi*, the diatom species used to

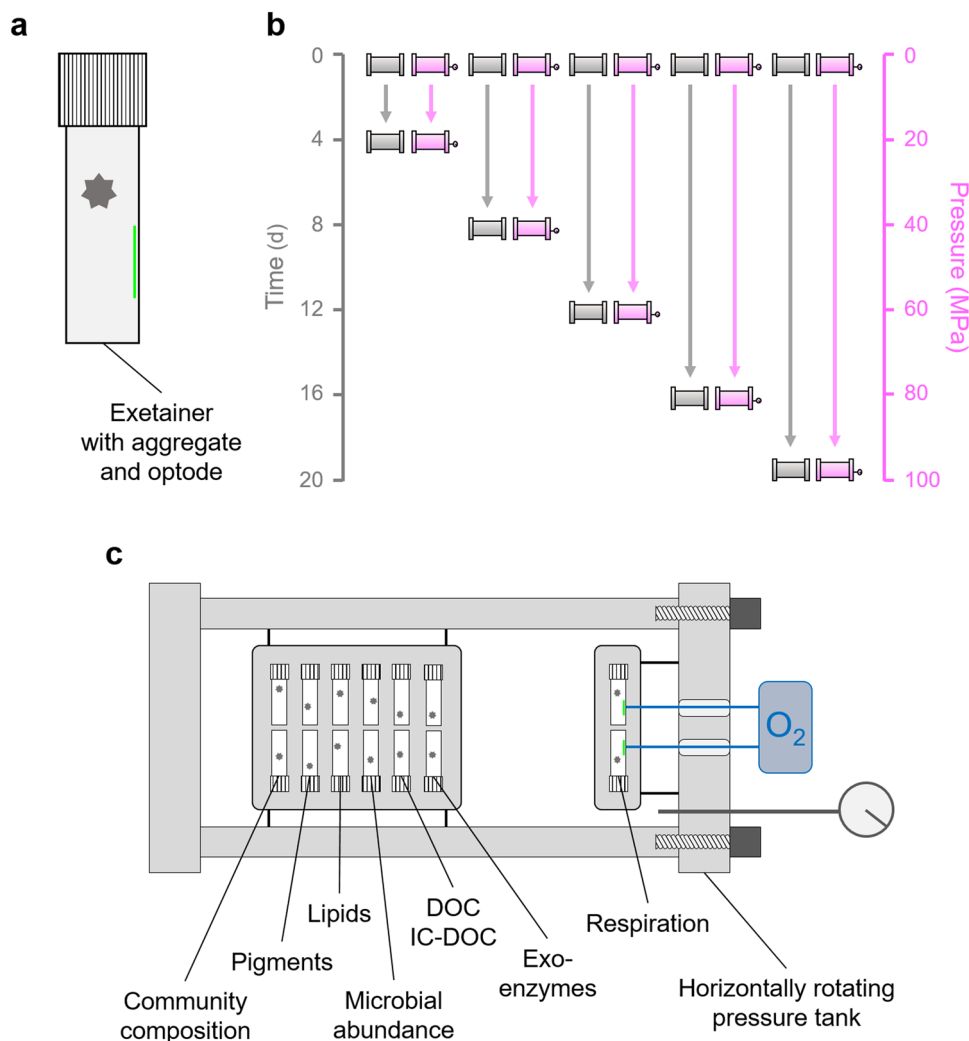


**Fig. 1 Experimental setup for high-pressure incubation of sinking diatom aggregates.** **a** Diatom aggregates (star symbol) were individually incubated in exetainers some of which were equipped with an oxygen-sensing optode (green line). **b** Exetainers with aggregates were distributed between 5 horizontally rotating control tanks (grey) and 5 pressure tanks (pink). Control tanks remained at atmospheric pressure throughout the 20-day incubation, while in the pressure tanks, hydrostatic pressure was incrementally increased to reach 100 MPa at the end of the incubation. One control and one pressure tank were opened after 4, 8, 12, 16, and 20 days to retrieve the aggregates. **c** Cross-section of a pressure tank. Aggregate respiration was continuously measured in those control and pressure tanks opened at the end of the incubation. The retrieved aggregates were analyzed for exoenzyme activities, ambient and intracellular dissolved organic carbon (DOC and IC-DOC), microbial abundance, diatom lipids and photopigments, and prokaryotic community composition.

produce the aggregates. Pure cultures of *S. marinoi* showed pronounced pressure-induced DOC leakage that paralleled the drop in intracellular DOC contents in extent and time (Supplementary Fig. 2a, b). In contrast, the intracellular contents of the photopigments chlorophyll *a* and fucoxanthin did not show a pressure-induced drop (Supplementary Fig. 2c, d). Thus, pressure-induced DOC leakage from *S. marinoi* applies to DOC in the vacuole and/or the cytosol, but not to membrane-associated pigments. DOC leakage from *S. marinoi* occurs during pressurization rather than depressurization as demonstrated in additional pressure and control experiments (Supplementary Fig. 3). In brief, when *S. marinoi* cells were first pressurized to 60 MPa in a rotating pressure tank, then allowed to settle inside the incubation flask for 3 h, and then depressurized, the leaked DOC was homogeneously distributed in the incubation flask rather than showing a concentration maximum overlapping with the *S. marinoi* cells at the bottom of the flask (see legend of Supplementary Fig. 3 for more details).

**Total carbon loss.** Organic carbon was lost from the aggregates via two pathways, respiration activity (Fig. 2) and DOC leakage (Fig. 3). Aggregate-associated respiration activities were converted to oxidative carbon loss by assuming a respiratory quotient of 0.8 (ref. 29). At a simulated sinking depth of 10 km, the cumulative carbon loss through respiration ( $C_{\text{loss}_{\text{Resp}}}$ ) was significantly lower in the pressure treatment (22–37% of the initial carbon contents of the aggregates) than in the control treatment (38–72%) (Student's *t*-test:  $t = 3.85$ ,  $df = 12$ ,  $p = 0.002$ ) (Fig. 4a). In contrast, the cumulative carbon loss through DOC leakage ( $C_{\text{loss}_{\text{Leak}}}$ ) was only noticeable in the pressure treatment. At a simulated sinking depth of 10 km,  $C_{\text{loss}_{\text{Leak}}}$  accumulated to a mean loss of 22.5% of the initial carbon contents of the aggregates (Fig. 4b).

At a simulated sinking depth of 4 km (i.e., approximately the average depth of the world oceans), the sum of  $C_{\text{loss}_{\text{Resp}}}$  and  $C_{\text{loss}_{\text{Leak}}}$ ,  $C_{\text{loss}_{\text{Total}}}$  had accumulated to higher values in the pressure than in the control treatment (i.e., ~40% and ~25%, respectively) (Student's *t*-test:  $t = 2.50$ ,  $df = 34$ ,  $p = 0.017$ ) (Fig. 4c).

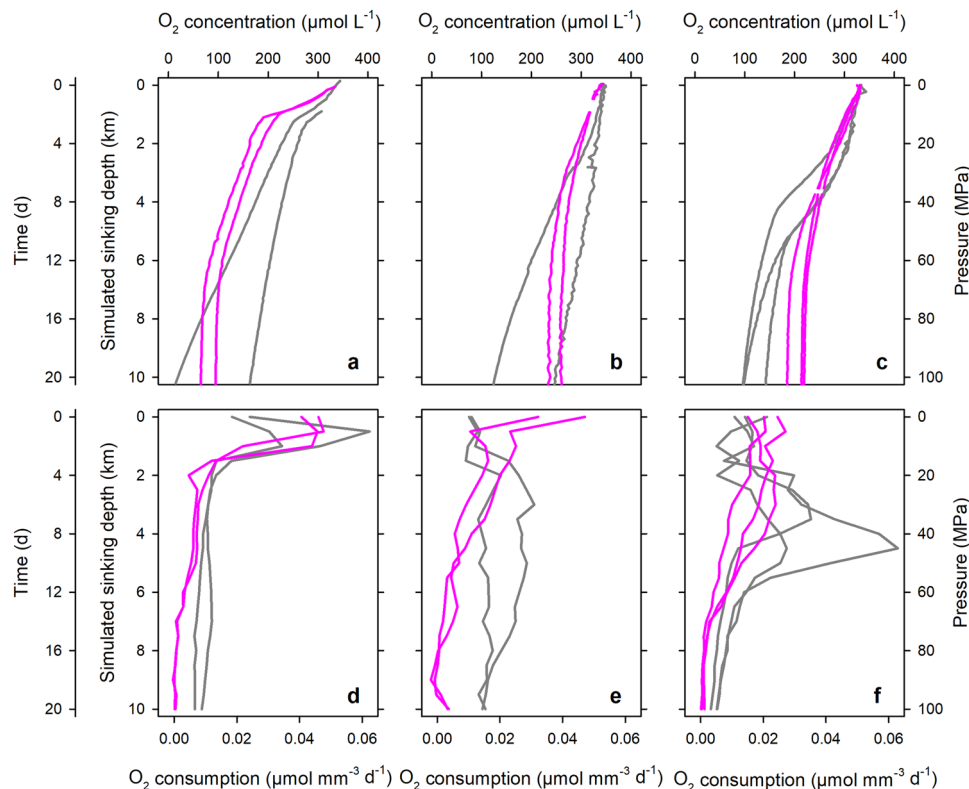


**Fig. 2 Aerobic respiration activity associated with sinking diatom aggregates.** Aggregates were individually incubated in rotating tanks at either atmospheric pressure (grey) or increasing pressure (pink). Increasing the pressure level simulates that the aggregates sink from the surface ocean (0 d  $\hat{=}$  0 km  $\hat{=}$  0.1 MPa) into a deep-sea trench (20 d  $\hat{=}$  10 km  $\hat{=}$  100 MPa). **a–c** Oxygen concentration measured in real time throughout the incubations. **d–f** Oxygen consumption rate per 1 mm<sup>3</sup> aggregate as calculated from the change in oxygen concentration over time. Aggregates were produced in three independent batches plotted separately in (**a+d**), (**b+e**), and (**c+f**). Gaps in oxygen concentration profiles are due to temporary technical failure.

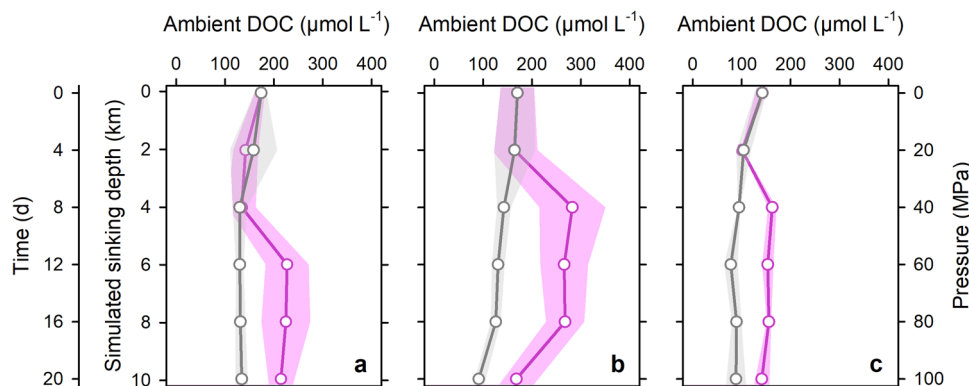


**Fig. 3 Leakage of dissolved organic carbon (DOC) from sinking diatom aggregates.** Aggregates were incubated at either atmospheric pressure (grey) or increasing pressure (pink). **a–c** DOC concentration in the seawater surrounding sinking aggregates produced in three independent batches. Means (circles)  $\pm$  standard deviation (shaded area) of (**a**)  $n = 3$ , (**b**)  $n = 9$ , and (**c**)  $n = 3$  replicate aggregates at the respective pressure level and in the respective treatment are shown.

This is consistent with weak reduction in respiration activity (Fig. 2d–f) and strong DOC leakage (Fig. 3a–c) at 0.1–40 MPa. At a simulated sinking depth of 10 km (i.e., the depth of a hadal trench), C loss<sub>Total</sub> had accumulated to the same value (i.e., ~55%) in the pressure and control treatments (Fig. 4c). This is consistent with complete inhibition of respiration activity (Fig. 2d–f) and very weak DOC leakage (Fig. 3a–c) at 60–100 MPa.

**Diatom lipidomics.** Diatom-specific storage and structural lipids as well as respiratory quinones were quantified to study pressure

effects on microbial lipid degradation and/or the lipid metabolism of potentially surviving diatoms (Fig. 5a–d). The contents of the storage lipids triacylglycerols (TAGs) and the respiratory ubiquinone (UQ<sub>10:10</sub>, nomenclature according to ref. <sup>30</sup>) decreased significantly with increasing pressure (Student's *t*-test of the slope of lipid versus pressure:  $t = -3.38$ ,  $df = 16$ ,  $p = 0.004$  and  $t = -2.31$ ,  $df = 16$ ,  $p = 0.035$ , respectively). The ubiquinone pool was essentially depleted at 40 MPa. In contrast, the contents of monogalactosyl-diacylglycerols (MGDGs), major lipids of the thylakoid membranes, and plastoquinone (PQ<sub>9:9</sub>) did not change with increasing pressure ( $t = 0.53$ ,  $df = 16$ ,  $p = 0.606$  and

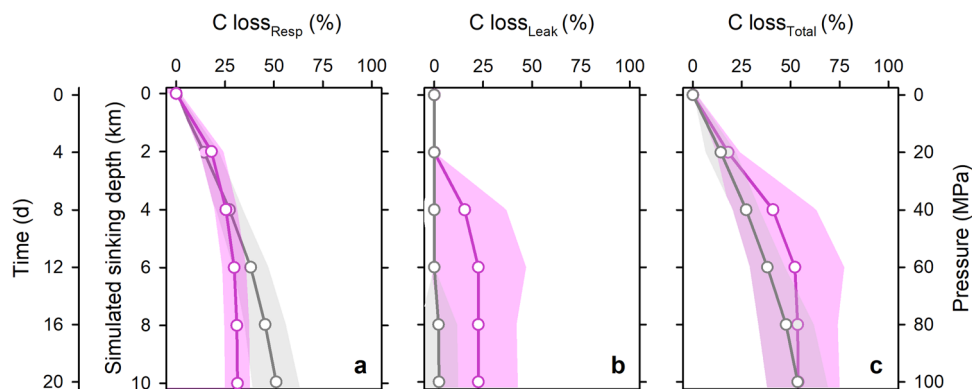


**Fig. 4 Cumulative carbon loss from sinking diatom aggregates.** Aggregates were individually incubated in rotating tanks at either atmospheric pressure (grey) or increasing pressure (pink). **a** Carbon loss through aerobic respiration ( $C\ loss_{Resp}$ ) as calculated from aerobic respiration rates (Fig. 2d, f) and a respiration quotient of  $RQ = 0.8$ . **b** Carbon loss through DOC leakage ( $C\ loss_{Leak}$ ) as calculated from the change in ambient DOC concentrations (Fig. 3a–c). **c** Total carbon loss ( $C\ loss_{Resp}$  plus  $C\ loss_{Leak}$ ) through  $C\ loss_{Resp}$  plus  $C\ loss_{Leak}$ . Carbon loss is expressed relative to the initial carbon content of the respective aggregate. Means (circles)  $\pm$  standard deviation (shaded area) of  $n = 7$  replicate aggregates ( $C\ loss_{Resp}$ ) and  $n = 15$  replicate aggregates ( $C\ loss_{Leak}$ ) are shown. Aggregates were produced in three independent batches that were pooled for this plot.

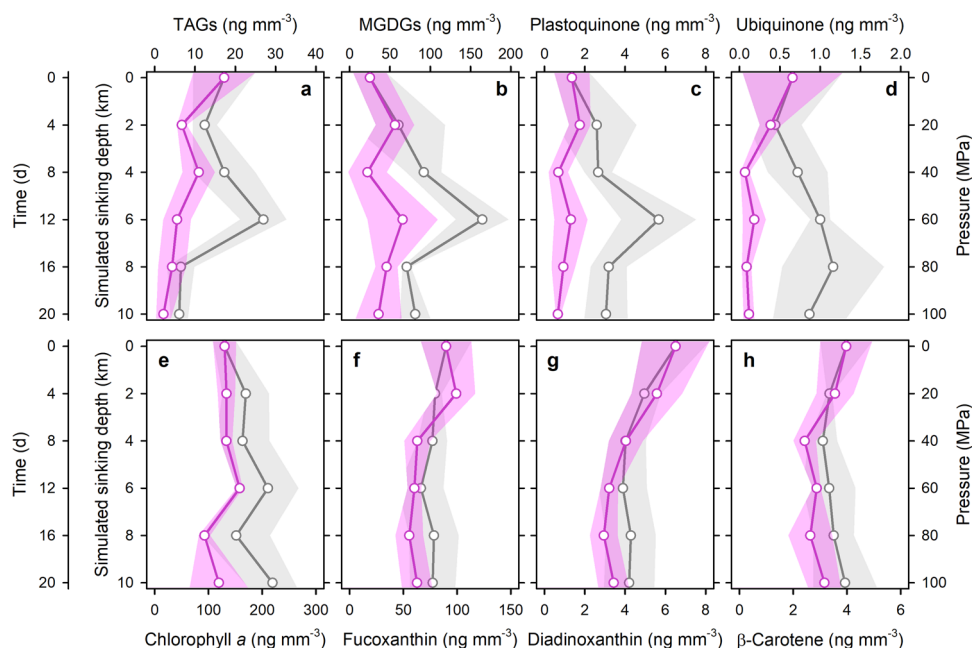


**Fig. 5 Lipid and photopigment contents in sinking diatom aggregates.** Aggregates were incubated at either atmospheric pressure (grey) or increasing pressure (pink). **a** TAGs=triacylglycerols, storage lipids that form cytosolic lipid droplets, **b** MGDGs=monogalactosyl-diacylglycerols, the major structural lipid in thylakoid membranes inside chloroplasts, **c** Plastoquinone ( $PQ_{9,9}$ )=a respiratory quinone integrated in chloroplast membranes, **d** Ubiquinone ( $UQ_{10,10}$ )=a respiratory quinone integrated in mitochondrial membranes. **e–h** Major diatom photopigments. Means (circles)  $\pm$  standard deviation (shaded area) of  $n = 3$  replicate aggregates are shown.

$t = -1.37$ ,  $df = 16$ ,  $p = 0.189$ , respectively). Instead, their contents markedly increased after 12 days of incubation at atmospheric pressure, as did the contents of TAGs.

For the fatty acids of two TAGs, the average unsaturation degree (AUD) was consistently higher in the pressure than in the control treatment (Supplementary Fig. 4a, b), but significant only for TAG- $C_{48}$  at 40–80 MPa (Student's  $t$ -test (one-tailed):  $p = 0.001$ – $0.030$ ). This observation is consistent with the concept of homeoviscous adaptation to high-pressure conditions. In contrast, the highly abundant MGDGs did not show higher AUD in the pressure treatment (Supplementary Fig. 4c, d).

**Diatom photopigments.** As expected for diatom-dominated aggregates, chlorophyll  $a$ , fucoxanthin, diadinoxanthin, and  $\beta$ -

carotene were the most abundant photopigments (Fig. 5e–h). Overall, pigment contents remained relatively stable during the 20-day incubation in darkness and were consistently lower at pressure levels  $\geq 60$  MPa than at atmospheric pressure, but these differences were not statistically significant (Student's  $t$ -test:  $p = 0.070$ – $0.655$ ). The contents of the chlorophyll  $a$  degradation products pheophytin  $a$  and pheophorbide  $a$  were very similar in the pressure and control treatment (Supplementary Fig. 5).

**Microbial abundance.** Diatom, bacterial, and viral abundances in the aggregates were  $>75000$ -fold,  $>25000$ -fold, and  $>1800$ -fold higher than in the ambient water, respectively (Fig. 6 and Supplementary Fig. 6). In the aggregates, the abundance of quantifiable diatom cells (*see* Materials & Methods) decreased



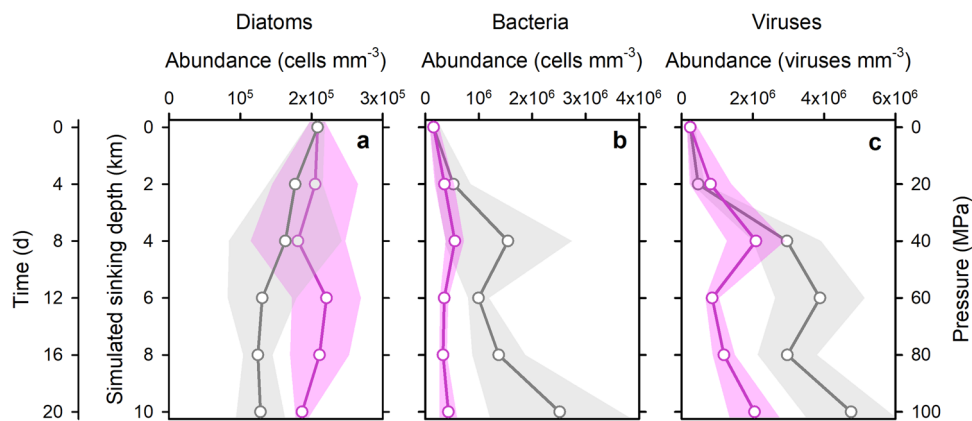


**Fig. 6 Total abundance of diatoms, bacteria, and viruses in sinking diatom aggregates.** Aggregates were individually incubated in rotating tanks at either atmospheric pressure (grey) or increasing pressure (pink). Diatoms (**a**) were counted in aggregates from batch 3, while bacteria (**b**) and viruses (**c**) were counted in aggregates from batch 2. Means (circles)  $\pm$  standard deviation (shaded area) of  $n = 3$  replicate aggregates are shown.

significantly in the control (Student's  $t$ -test of slope of abundance versus pressure:  $t = -3.06$ ,  $df = 16$ ,  $p = 0.008$ ), but not in the pressure treatment ( $t = -0.25$ ,  $df = 16$ ,  $p = 0.807$ ), indicating reduced diatom degradation with increasing pressure (Fig. 6a). With estimated carbon contents of 1.28–1.46 pmol C per cell<sup>31</sup>, *S. marinoi* contributed ~43–49% to the initial carbon contents of the aggregates. Bacterial abundance increased significantly in the control ( $t = 3.75$ ,  $df = 16$ ,  $p = 0.002$ ) and moderately in the pressure range of 0.1–40 MPa ( $t = 3.52$ ,  $df = 7$ ,  $p = 0.010$ ) (Fig. 6b). At pressure levels of  $\geq 40$  MPa, however, bacterial abundance remained unchanged ( $t = -1.05$ ,  $df = 10$ ,  $p = 0.317$ ), indicating inhibition of bacterial growth. Viral abundance increased significantly in the control ( $t = 5.99$ ,  $df = 16$ ,  $p < 0.001$ ) and moderately in the pressure treatment ( $t = 2.62$ ,  $df = 16$ ,  $p = 0.019$ ) (Fig. 6c). With estimated carbon contents of 2.5 fmol C per cell<sup>32</sup> and 0.0046 fmol C per virus particle<sup>33</sup>, bacteria and viruses contributed 0.07 and 0.0002%, respectively, to the initial carbon contents of the aggregates.

**Microbial community composition.** The microbial communities associated with 41 individual diatom aggregates incubated under pressure and control conditions were analyzed via 16S rRNA gene amplicon sequencing. From the 765 amplicon sequence variants (ASVs) generated, 12 were identified as belonging to Cyanobacteria, the most abundant of which (>98% of all cyanobacterial sequences) belonged to the chloroplast of the diatom genus *Skeletonema* (BLAST). The relative abundance of ASVs belonging to Archaea was always  $\leq 0.04\%$ ; therefore, we focus our discussions on bacteria as the prokaryotes mainly associated with diatom aggregates. For the subsequent analysis, both the chloroplast and the mitochondrial ASVs were removed from the data set. Most bacterial ASVs belonged to three classes: Alphaproteobacteria, Gammaproteobacteria, and Bacteroidia (Fig. 7a). Within these classes, ASVs were assigned to 25, 31, and 23 different families, respectively. The most abundant families were Rhodobacteriaceae (Alphaproteobacteria), Alteromonadaceae (Gammaproteobacteria), and Flavobacteriaceae (Bacteroidia).

Bacterial community composition changed gradually during the incubation under both pressure and control conditions (Fig. 7b), with significant differences between the two treatments (PERMANOVA,  $R^2 = 0.21$ ,  $p < 0.001$ ). Community compositions started to diverge mainly at  $\geq 60$  MPa between the control- and pressure-treated aggregates (Fig. 7c).

Few families (6 out of the 28 most abundant families) showed consistent increases in relative abundance with increasing pressure (Supplementary Fig. 7a), of which only Devosiaceae

(Alphaproteobacteria) was generally abundant in the aggregates (Supplementary Fig. 7b). Few families (7 out of 28) showed consistent decreases in abundance with increasing pressure (Supplementary Fig. 7a), of which, for example, Rhodobacteriaceae (Alphaproteobacteria) and Flavobacteriaceae (Bacteroidia) were generally abundant (Supplementary Fig. 7b). Most families (15 out of 28) showed fairly stable relative abundances with increasing pressure (Supplementary Fig. 7a), of which Alteromonadaceae (Gammaproteobacteria) were generally abundant (Supplementary Fig. 7b).

## Discussion

**Carbon loss versus carbon preservation.** Extensive degradation of sinking particles due to microbial activities and metazoan grazing takes place in the epi- and mesopelagic zone of the ocean<sup>4–7</sup>. The vertical carbon flux is thus strongly attenuated in these surface layers<sup>9</sup>. Our study demonstrates that the low and nearly unattenuated carbon flux in deeper layers is, at least in part, an effect of increasing hydrostatic pressure that gradually reduces microbial particle degradation. According to our results, complete inhibition of microbial particle degradation is achieved at pressure levels at depths of 6 km and greater (Fig. 8). The inhibitory effect of pressure on microbial particle degradation was mediated by progressive inhibition of aerobic respiration, while exoenzymatic processes were differentially affected by pressure (i.e., stimulated versus reduced versus neutral). This discrepancy might be explained by the pressure-induced impairment of the membrane-associated electron transport in aerobic respiration<sup>19</sup> versus the limited denaturing effect of similar pressure levels on proteins and enzymes<sup>20</sup>. As a caveat, subtle modifications of pressure on enzyme conformation can alter the catalytic efficiency, but these effects can be neutral, inhibitory, or stimulatory<sup>34</sup>, as also observed in our study.

In the natural environment of the ocean, the diverse factors that affect particle degradation and thus carbon preservation likely act in concert. Particle-attached microorganisms adapted to surface-water conditions sink through relatively steep temperature gradients in low and middle latitudes and the large pressure gradient with depth in all global oceans (Fig. 8), which both progressively reduce microbial metabolism and thus microbial particle degradation. Additionally, the abundance of zooplankton grazing on sinking particles decreases with depth<sup>26</sup>, which further reduces particle degradation in the deep ocean. Together, these biotic and abiotic factors inhibiting particle degradation enable the sequestration flux of particles below 1 km depth<sup>35,36</sup>. Once particles reach below 1 km depth, particulate organic carbon

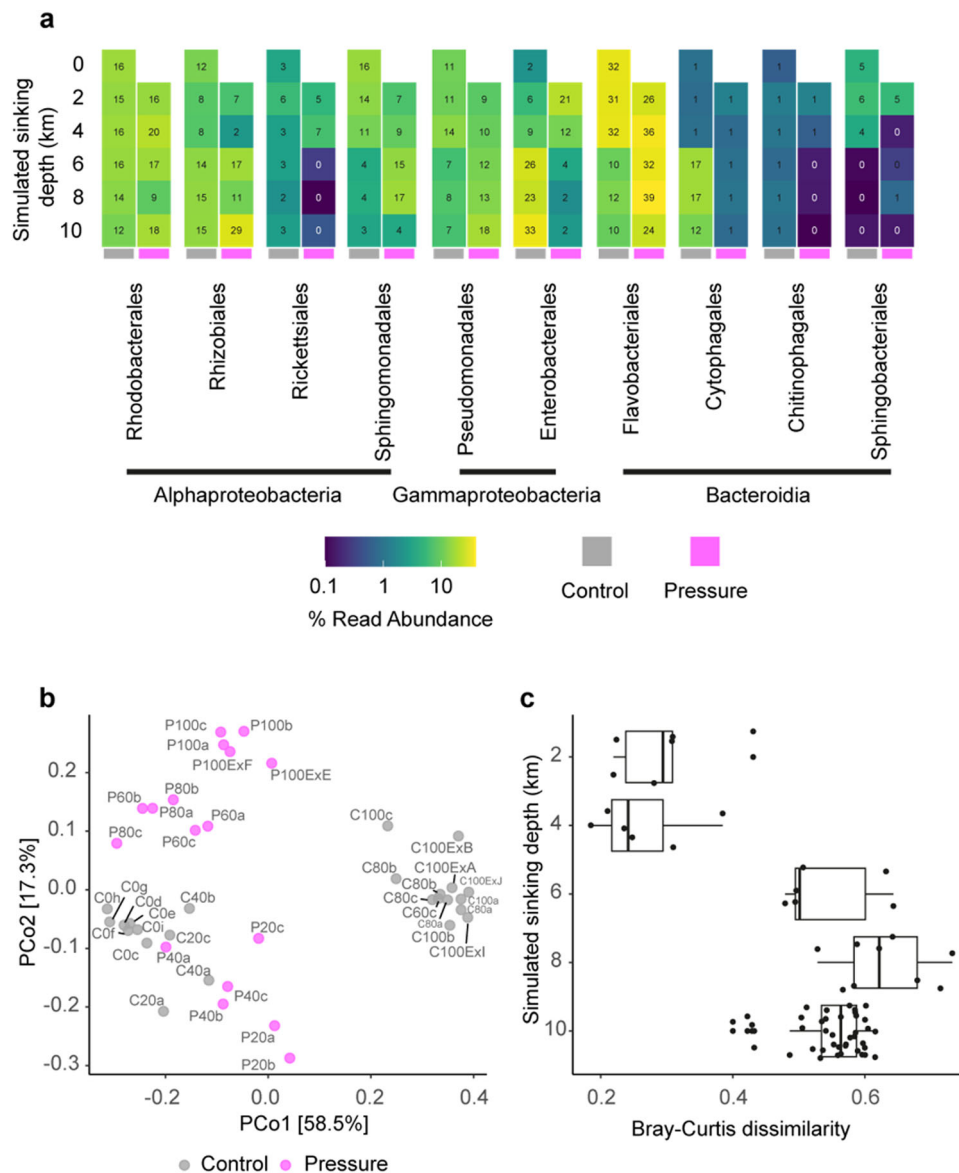


**Fig. 7 Prokaryotic community analysis of sinking diatom aggregates.** **a** Heatmap of 16 S rRNA gene-based prokaryotic community composition in diatom aggregates incubated at either atmospheric pressure (grey) or increasing pressure (pink). Means of  $n = 3$  replicate aggregates are shown ( $n = 7$  for C0 samples collected at  $t_0$ ). **b** Principal Coordinates Analysis (PCoA) based on the Bray-Curtis dissimilarity metric of 705 ASVs and 41 aggregates. C and P notations mark aggregates from the control and pressure treatment, respectively; numbers give the pressure level in MPa; lower letters denote replicates. No initial data transformation has been applied. The relative contribution (eigenvalue) of each axis to the total inertia in the data is indicated in percent in the axis titles. **c** Bray-Curtis dissimilarity between control- and pressure-treated aggregates. Boxes represent the interquartile ranges, the line within the box the median, and the whiskers extend to the minimum and maximum values within 1.5 times the interquartile range. Dots show all pairwise comparisons.

(POC) and carbon dioxide potentially produced during POC mineralization are trapped in the slowly circulating deep ocean water for millennia<sup>37</sup>. Particle-fed carbon sequestration is mediated by POC deposition and subsequent burial of a minor fraction in the seabed<sup>38</sup>.

Pressure-induced DOC leakage from diatom aggregates discovered in our study suggests significant carbon loss already during the descent to depth (Fig. 8). The aggregate-forming diatom *Skeletonema marinoi* loses its entire intracellular DOC at pressure levels >60 MPa and thus approximately half of its total carbon contents<sup>31</sup>. The underlying mechanism remains to be unraveled, but likely involves impaired integrity and functioning of cell membranes, as otherwise known for bacteria<sup>19,20</sup>, together with the pressure-induced volumetric compression of water. For

particle-attached bacteria, DOC leakage from the diatoms might facilitate oxidative carbon mineralization. However, DOC leakage occurs at pressure levels that reduce or even inhibit the respiration activity of surface-adapted, particle-attached bacteria. Eventually, the diffusion of leachates into the ambient water means a loss of organic substrates for particle-attached bacteria.

At first glance, DOC leakage seems to reduce the amount of particle-associated carbon that can be sequestered in the deep ocean. However, DOC leakage was observed only at simulated sinking depths of 4 km (diatom aggregates) and 6 km (healthy diatom cultures), which is well below the sequestration depth of 1 km. In natural settings, sinking diatom aggregates may thus fuel the persistent DOC pool in the deep ocean<sup>39</sup>, especially through the leakage of polysaccharides, such as laminarin and

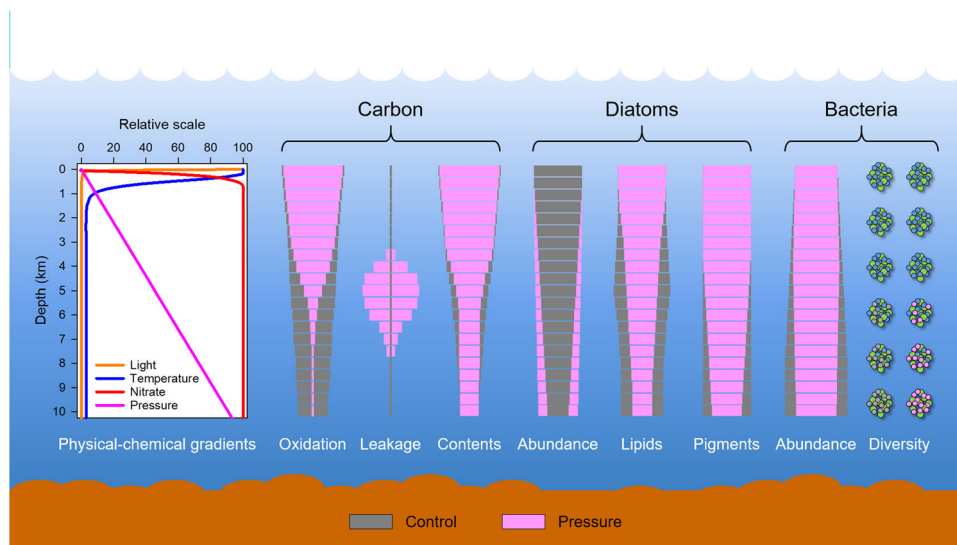


**Fig. 8** Effects of hydrostatic pressure on sinking diatom aggregates in the ocean. Aggregates sink through relatively steep gradients of light, temperature, and nitrate and the long-stretched gradient of hydrostatic pressure. High-pressure levels reduce oxidative carbon mineralization, but trigger carbon leakage, which together result in a conspicuous carbon loss from the aggregates at mid-depth, but no further carbon loss at greater depth. High-pressure levels reduce the microbial degradation of diatoms and cause moderate decreases in diatom lipid and photopigment contents. High-pressure levels prevent aggregate-associated bacteria from growing and cause significant shifts in bacterial community composition. Vertical gradients are stylized.

fucoidan<sup>40–42</sup>. In the surface ocean, laminarin can be turned over quickly<sup>40</sup>. At 4–6 km depth, however, laminarin leaking from diatom cells may evade microbial degradation because of the pressure sensitivity of laminarase observed in our study. Fucoidan and other complex polysaccharides are generally resilient to enzymatic degradation<sup>43,44</sup>. However, given the general substrate scarcity in the deep ocean, bacterial communities may show adaptations to exploit the pressure-induced DOC leakage from sinking particles<sup>45</sup>.

Interestingly, the observed pressure-induced DOC leakage from sinking particles supports previous indications of the existence of a substantial pool of bioavailable DOC ( $\sim 1\text{--}2\ \mu\text{mol L}^{-1}$ ) at water depths  $>3$  km from global ocean circulation models<sup>46</sup>. In that study, dissolution of the sinking particles by viral cell lysis and prokaryotic enzymatic activity were suggested as the source of bioavailable DOC in the deep ocean. However, our results show that viral production on particles was significantly lower in the pressure treatment than in the control treatment, leaving pressure-induced DOC leakage as a more likely source of bioavailable DOC in the deep ocean.

**Organic matter composition.** The above findings imply that increasing pressure levels differentially regulate oxidative carbon mineralization (reduction or inhibition) and DOC leakage (stimulation). Therefore, pressure exposure modifies the organic matter composition of sinking particles in favor of organelle- and/or membrane-associated organic compounds and at the expense of intracellularly-dissolved organic compounds. In the diatom aggregates studied here, the former compounds comprise photopigments and lipids, which showed less dramatic losses than the organic compounds dissolved in the vacuole and the cytosol of *S. marinoi* cells (Fig. 8). Aside from their subcellular location, the molecular complexity and thus degradability of individual organic compounds are likely to determine the change in organic matter composition of particles sinking through the vertical pressure gradient of the ocean<sup>47</sup>.

The photopigments of diatoms are anchored to membranes inside the chloroplast and have a relatively complex molecular

structure. Thus, it is not surprising that increasing pressure levels resulted in only moderate losses in photopigment contents that may have occurred through leakage or bacterial degradation. Additionally, pressure exposure did not alter the contents of the chlorophyll degradation products pheophytin and pheophorbide, further substantiating that pigment loss through pressure-induced degradation processes were not important. This finding raises questions into the factors that lead to systematically lower pigment contents of the diatom aggregates at high versus low-pressure levels. Possibly, *S. marinoi* survives dark, cold, and high-pressure conditions and degrades its own photopigments to meet dissimilatory and/or assimilatory demands. External stress factors are known to induce autophagy of cellular components in diatoms<sup>48,49</sup>. Even at highest pressure levels, however, the cellular contents of photopigments remained substantial, which makes them suitable biomarkers even in the deep ocean.

Among the studied diatom lipids, MGDGs, PQ<sub>9,9</sub>, and UQ<sub>10,10</sub> are organelle- and membrane-associated, while TAGs are located in the cytosol or the vacuole. The generally observed decrease in lipid contents in the pressure treatment may be due to bacterial lipid degradation of diatom cells that are compromised by exposure to pressure. However, mechanical damage of diatom cells was not observed under a microscope. Instead, a more likely explanation is lipid metabolism by the diatoms themselves, assuming that they survive the pressure treatment. Stressed diatoms are known to sacrifice membrane lipids for TAG production to feed minimal dark respiration activity under prolonged darkness<sup>49</sup>. TAGs are then shuttled as lipid droplets into the vacuole where they will be degraded<sup>48</sup>. Diatoms are also known to re-allocate lipid resources during the formation of resting stages<sup>50</sup>. TAG contents of pressure-treated aggregates actually started decreasing before DOC leakage was stimulated and respiration activity was inhibited, suggesting that the diatoms might still have been metabolically active at that time. The subsequently very low UQ<sub>10,10</sub> contents in pressure-treated diatom aggregates is consistent with the minimal respiration activity of diatom resting stages<sup>51</sup>. While nitrogen limitation is a well-known trigger of resting stage formation<sup>50,52,53</sup>, pressure may additionally serve as a reliable environmental cue. However,



*S. marinoi* resting stages were not observed in the diatom aggregates studied here, potentially because *S. marinoi* forms resting cells that are morphologically very similar to vegetative cells<sup>54</sup>. Diatom resting stages can be a major component of the vertical carbon flux in the ocean<sup>55–57</sup> and thus their organic matter composition may leave a lasting imprint in the sediment record of the deep ocean.

Differences in organic matter composition of the aggregates may also arise, if diatoms survive the control treatment, but die in the pressure treatment. Surviving diatoms may show physiological responses to the dark and cold conditions that cannot be at work in dead diatoms. For example, *S. marinoi* seems to increase TAG production in response to dark stress (Fig. 5a), which substantially enhances the difference in TAG contents between control- and pressure-treated aggregates. The same might be true for the other diatom lipids identified and quantified here. It is thus necessary to specifically address the survival potential and the possible physiological adaptations of diatoms to high-pressure conditions in future studies.

**Microbial community composition.** The pressure-inhibited oxidative carbon mineralization paralleled the halted decrease in diatom abundance with simulated sinking depth (Fig. 8). Additionally, the pressure-stimulated DOC leakage was recognizable from the presence of transparent-looking diatom cells. Based on light microscopy, pressure exposure neither crushed the diatom cells, nor resulted in the loss of chloroplasts, which is consistent with the relatively high photopigment contents of pressure-exposed aggregates. Thus, finding healthy-looking diatom cells and/or their resting stages in the deep ocean may be plausible<sup>10,58,59</sup> potentially even in hadal trenches. It remains to be investigated, if this applies also to other microbial eukaryotes that are associated with sinking particles, such as coccolithophores, dinoflagellate cysts, foraminifera, and fungi<sup>6,29,60,61</sup>.

The pressure-inhibited oxidative carbon mineralization was also consistent with the lack of bacterial net growth. Bacterial abundance remained relatively stable down to a simulated sinking depth of 10 km, which means that bacterial growth at most compensated bacterial mortality (Fig. 8). Turnover of bacterial populations resulted in a gradual, but significant shift in bacterial community composition. The majority of bacterial families responded to increasing pressure with only subtle changes in relative abundance, which might suggest that they harbor abundant piezotolerant representatives. In contrast, relatively few bacterial families showed consistent increases or decreases in relative sequence abundance, which might suggest that they harbor abundant piezotolerant/piezophilic and piezosensitive representatives, respectively. This preliminary interpretation of the relative abundance data aligns well with recent observations made in natural deep-sea water<sup>16</sup>. In particular, the pressure sensitivity of Alteromonadaceae appears to be confirmed by our data. However, our 16S rDNA-based community analysis provides compositional data and the apparent increase in abundance of one taxon might simply result from the decrease in abundance of another taxon. This leaves open which of the two taxa showed a change in *absolute* abundance with increasing pressure – or if even both taxa changed in *absolute* abundance simultaneously. Hence, changes in relative abundance may simply indicate which bacterial taxa coped better or worse with increasing pressure levels than others. These trends may at best give hints to which bacterial families potentially harbor pressure-adapted representatives. Classification as piezophilic, piezotolerant, and piezosensitive should be validated by experimentally-determined pressure optima for growth of bacterial isolates.

Generally, piezophilic and piezosensitive bacteria attached to sinking particles might be selected for and against, respectively, by the vertical pressure gradient in the ocean, while piezotolerant bacteria probably remain unaffected. In our simulation experiment, piezophilic bacteria were obviously not significantly enriched within the diatom aggregates as otherwise oxidative carbon mineralization would have been resumed in the hadal pressure range of 60–110 MPa. Thus, piezophilic bacteria were either absent in the surface-derived communities, or rare and not exposed to favorable growth conditions during the incubations. In natural settings, most particle-attached bacteria seem to be piezotolerant and only survive the high-pressure conditions of the deep ocean, but do not thrive better at high than at low hydrostatic pressure<sup>16</sup>. Hence, deep-sea sediments might be seeded with surface-derived, particle-attached bacterial populations that can cope with high pressure levels at least to some extent<sup>62</sup>. In accordance with this view, the high microbial carbon turnover discovered in hadal sediments<sup>63–65</sup> indicates, amongst others, that microbes which are at least piezotolerant are present and active<sup>66</sup>.

## Materials and methods

**Diatom aggregates.** For each of three independent incubation experiments, a new batch of model diatom aggregates was produced by mixing 1 part stationary-phase diatom culture and 9 parts natural seawater in 500 mL glass bottles<sup>67</sup>. The aggregate-forming diatom *Skeletonema marinoi* (CCMP1332) was obtained as an axenic culture from NCMA (Bigelow, U.S.A.) and cultured in L1 medium<sup>68</sup>. Natural seawater (35 psu) was collected in the Kattegat off the coast of Denmark at 28 m depth, 3 µm-filtered to remove phytoplankton and keep the bacterioplankton, and stored in darkness until used. The glass bottles with the diatom-seawater mixture were mounted on a plankton wheel and rotated at 2 rpm. Near-spherical aggregates (diameter = ~2–3 mm) composed of *S. marinoi* and the natural microbial community of surface seawater formed within 1–2 days and were used for experiments within ~7 days. One day before each incubation experiment, the aggregates were gently transferred to 500 mL of 0.22 µm-filtered and autoclaved seawater (30 psu) prepared from Red Sea salt (Red Sea Aquatics Ltd., Cheddar, U.K.), henceforth referred to as RSW30.

For normalization of measured variables, the volume of each aggregate was determined by image analysis (ImageJ, NIH, Bethesda, U.S.A.) prior to experiments<sup>14</sup>. The aggregates from batch 1, 2, and 3 had volumes of  $7.9 \pm 3.9$  (50),  $3.7 \pm 2.6$  (259), and  $4.0 \pm 2.5$  (459) mm<sup>3</sup> (mean ± standard deviation (total number of aggregates)), respectively. For each of the three batches of aggregates, the total organic carbon content of ≥20 randomly selected aggregates of known volume was determined on a Na 1500 elemental analyzer (Fisons, Loughborough, U.K.). The aggregates from batch 1, 2, and 3 contained  $441 \pm 58$ ,  $517 \pm 137$ , and  $599 \pm 203$  nmol C mm<sup>-3</sup> (mean ± standard deviation), respectively. The mean volumetric carbon contents were used to estimate the carbon contents of all other aggregates used in the experiments from their individual volume as determined by image analysis.

## Experimental design

**Rotating incubation tanks.** Pressure incubations at up to 100 MPa were conducted in a set of 5 cylindrical, stainless steel tanks with inner dimensions of 100–160 mm in diameter and 400–630 mm in length (Dustec GmbH, Wismar, Germany) (Fig. 1). The tanks were pressurized with a pneumatic-driven pump (Dustec GmbH, Wismar, Germany) and horizontally rotated at 5 rpm on custom-made roller tables. Control incubations at 0.1 MPa were conducted in 5 custom-made cylindrical tanks with inner dimensions

of 100–160 mm in diameter and 200–400 mm in length. These tanks were made of acrylic rendered opaque by wrapping with black tape and horizontally rotated at 5 rpm on custom-made roller tables. Visual inspection in a parallel tank left transparent confirmed that the rotation speed maintained aggregates in suspension throughout the experiments.

**Incubation vials.** Inside the rotating tanks, the aggregates were incubated individually in 3- or 6 mL glass exetainers (Labco Ltd., Lampeter, U.K.) (Fig. 1a). The flexible septum cap of the exetainers efficiently compensates the compression of water by ~4% at 3 °C and 100 MPa<sup>69</sup>. For cleaning and sterilization, the exetainers were rinsed with deionized water, soaked in 1% HCl for 5–10 min, and rinsed again with deionized water. Before adding the aggregates, the exetainers were filled with temperature- and air-equilibrated RSW30.

**Time schedule.** All incubation experiments were conducted at 3 °C and in the dark. In the 5 pressure tanks, the complete pressure history of aggregates sinking from the surface ocean (i.e., 0 km  $\triangleq$  0.1 MPa) into a deep-sea trench (i.e., 10 km  $\triangleq$  100 MPa) was simulated (Fig. 1b). The speed at which pressure was increased over time was guided by the sinking speed of model diatom aggregates of  $\sim 500 \text{ md}^{-1}$  as previously determined<sup>14</sup>. The pressure level was increased in steps of 5 MPa every day. After reaching 20 MPa in all pressure tanks, one of the pressure tanks was depressurized and opened to retrieve the aggregate samples. In the remaining pressure tanks, the stepwise increase in pressure was continued until one tank after the other was depressurized after reaching pressure levels of 40, 60, 80, and 100 MPa. In the 5 control tanks, the pressure level was always left at 0.1 MPa, while all remaining incubation conditions and sampling time points were the same as in the pressure tanks. The last pressure and control tanks to be opened were the ones in which the continuous oxygen measurements were made (Fig. 1c).

Replicate aggregate samples were incubated in pressure and control tanks for measuring aerobic respiration activity, exoenzyme activities (Supplementary Methods), ambient and intracellular dissolved organic carbon (DOC) analysis, quantification of microbial abundance in the aggregates and the surrounding seawater, diatom lipid and photopigment analysis, and prokaryotic community analysis (Fig. 1c, Supplementary Table 1). Where applicable, aggregates and/or the surrounding seawater were sampled as t0 samples immediately before the experimental incubations were started.

**Respiration activity.** Aerobic respiration activity associated with diatom aggregates was measured to quantify oxidative carbon mineralization. To this end, oxygen concentration was continuously monitored in the exetainers throughout the 20-day incubations as described in ref. <sup>14</sup>. In brief, 4 exetainers in one pressure and control tank each were equipped with an internal oxygen-sensing optode foil that was interrogated by an oxygen meter (FireSting, PyroScience, Aachen, Germany) via a fiberoptic cable that was externally mounted on the exetainer to face the optode foil. The fiber optic cable penetrated the lid of the respective tank and was connected to the oxygen meter mounted on top of the lid. The signals measured by the oxygen meter were transferred to a PC via a USB cable with an integrated slipring thereby allowing continuous rotation of the tanks.

The custom-made optode foil of each exetainer was calibrated in temperature- and air-equilibrated RSW30 before each incubation experiment. An increase in hydrostatic pressure results in a slight increase in temperature and oxygen solubility and a decrease in optode sensitivity by ~3% per 10 MPa<sup>70</sup>. The

combined effect of these physical-chemical changes on the optode signals was compensated for by calculations described in ref. <sup>14</sup>.

For each incubation experiment, one aggregate each was added to 4–6 optode exetainers filled with temperature- and air-equilibrated RSW30. Two additional optode exetainers did not receive an aggregate and served as negative controls in which the physical-chemical effects on the optode signals were recorded. The pressure and control tanks received 2–3 exetainers with and one exetainer without an aggregate each. In total, 7 individual aggregates from batch 1, 2, and 3 were incubated in the pressure tank and seven in the respective control tank. After closing the tanks, optode signals were recorded every 5 min. Respiration rates were calculated from the linear regression of the daily decrease in the corrected oxygen concentrations and expressed per 1 mm<sup>3</sup> of aggregate. The cumulative carbon loss from the aggregates through aerobic respiration was calculated by adding up the daily respiration rates and applying a respiratory quotient of 0.8 (ref. <sup>29</sup>).

**Dissolved organic carbon.** Since carbon loss from the aggregates may also occur through the release of dissolved organic carbon (DOC), bulk DOC concentrations were monitored in both the seawater surrounding the aggregates and inside the aggregate-associated microbial cells. For aggregates from batch 1, the designated exetainers were placed upright for a few minutes to let the aggregate sink to the bottom. The top 4 mL of seawater in the exetainer were filtered through a pre-combusted 0.3  $\mu\text{m}$  glass-fiber filter (GF75, Advantec MFS Inc., Dublin, U.S.A.) and the filtrate collected in an acid-washed centrifugation tube (15 mL), which was stored at 4 °C until analysis (= ambient DOC sample). The aggregate was carefully transferred into an acid-washed centrifugation tube (15 mL) filled with 5 mL deionized water. For extraction of DOC contained inside the aggregate-associated microbial cells (i.e., intracellular DOC = IC-DOC), the aggregate sample was first snap-frozen in liquid nitrogen and then thawed in a water bath kept at 80–90 °C. Repeating this freeze-thaw cycle 2–3 times destroys microbial cells and makes them release all IC-DOC<sup>71</sup>. The extracted sample was centrifuged at 3000 g for 5 min and 4 mL of the supernatant were filtered through a 0.3  $\mu\text{m}$  glass-fiber filter (GF75). The filtrate was collected in an acid-washed centrifugation tube (15 mL), which was stored at 4 °C until analysis (= IC-DOC sample). The collective IC-DOC contents of aggregate-associated microbial cells was calculated from the concentration difference in the IC-DOC sample and the ambient DOC sample and expressed per sample volume and per 1 mm<sup>3</sup> of aggregate. All DOC samples were analyzed on a Total Organic Carbon (TOC) analyzer (TOC-L, Shimadzu Europa GmbH).

The observed pressure-induced release of DOC from the aggregates (i.e., DOC leakage) motivated a supplementary incubation experiment with the *S. marinoi* pure culture. This experiment had the same overall design as the aggregate experiments and served to identify *S. marinoi* as the likely source of the pressure-induced DOC leakage from aggregates. One part of stationary-phase diatom culture was mixed with 4 parts of RSW30 to arrive at an *S. marinoi* abundance of  $\sim 5 \times 10^5$  cells mL<sup>-1</sup>. This cell suspension was distributed between 11 60 mL polyethylene flasks that were incubated in 5 pressure and 5 control tanks, while one flask was immediately sacrificed and served as the t0 sample. After sample retrieval, the cell suspension in each flask was filtered through a 0.3  $\mu\text{m}$  glass-fiber filter (GF75) and 3 mL of the filtrate were stored at 4 °C until analysis (= ambient DOC sample). The filter containing the *S. marinoi* biomass was inserted into an acid-washed centrifugation tube (15 mL) to which 10 mL of deionized water were added for IC-DOC extraction through freeze-thaw cycling. The extracted

sample was centrifuged at 3000 g for 5 min and 4 mL of the supernatant were filtered through a 0.3 µm glass-fiber filter (GF75). The filtrate was collected in an acid-washed centrifugation tube (15 mL), which was stored at 4 °C until analysis (= IC-DOC sample). The IC-DOC contents of the *S. marinoi* culture was calculated from the concentration difference in the IC-DOC sample and the ambient DOC sample and expressed per sample volume.

**Diatom lipidomics.** For lipid analysis, 3 replicate aggregates from each treatment and sampling time point were individually transferred to 5-mL centrifugation tubes and stored at -20 °C until processed. Lipids were ultrasonically extracted from triplicate individual aggregates following a modified Bligh & Dyer protocol<sup>72</sup> using a monophasic mixture of methanol, dichloromethane, and 50 mM phosphate buffer at pH 7.4 (2:1:0.8, v-v-v). 1,2-diheneicosanoyl-*sn*-glycero-3-phosphocholine (C21-PC) was used as internal standard. The total lipid extracts (TLE) were dried under a stream of N<sub>2</sub> and stored at -20 °C until measurement. Lipids were analyzed by injecting TLE aliquots dissolved in methanol:dichloromethane (9:1, v-v) on a Dionex Ultimate 3000 high-performance liquid chromatography (HPLC) system connected to a Bruker maXis Ultra-High Resolution quadrupole time-of-flight tandem mass spectrometer (qToF-MS) equipped with an ESI ion source operating in positive mode (Bruker Daltonik, Bremen, Germany). The mass spectrometer was set to a resolving power of 27,000 at *m/z* 1,222 and every analysis was mass-calibrated by loop injections of a calibration standard and correction by lock mass, leading to a mass accuracy of better than 1-3 ppm<sup>73</sup>. Analyte separation was achieved using reversed phase HPLC on an Acquity UPLC BEH C<sub>18</sub> column (1.7 µm, 2.1 × 150 mm, Waters, Eschborn, Germany) maintained at 65 °C<sup>74</sup>. Analytes were eluted at a flow rate of 0.4 mL min<sup>-1</sup> using linear gradients of methanol: water (85:15, v-v, eluent A) to methanol: isopropanol (50:50, v-v, eluent B) both with 0.04% formic acid and 0.1% NH<sub>3</sub>. The initial condition was 100% A held for 2 min, followed by a gradient to 15% B in 0.1 min and a gradient to 85% B in 18 min. The column was then washed with 100% B for 8 min. Lipids were identified by retention time as well as accurate molecular mass and isotope pattern match of proposed sum formulas in full scan mode and MS<sup>2</sup> fragment spectra. Integration of peaks was performed on extracted ion chromatograms (EICs) of ±10 mDa width and included the [M+H]<sup>+</sup>, [M+NH<sub>4</sub>]<sup>+</sup>, and [M+Na]<sup>+</sup> ions using Data Analysis™ software (Bruker Daltonik, Bremen, Germany). Lipid abundances were corrected for response factors of commercially available standards in external standard curves. A Monogalactosyldiacylglycerol (MGDG) standard from Avanti Polar Lipids (Alabaster, AL, U.S.A.) was used to correct MGDG. Quinone abundances were corrected for the relative response of a ubiquinone (UQ; UQ<sub>10:10</sub> for UQs, and PQs) standard (Sigma-Aldrich, St. Louis, MO, U.S.A.). Triacylglycerols (TAGs) were corrected using a series of individual standards from Nu-Check-Prep (Elysian, MN, U.S.A.). TAG response factors were based on the equivalent carbon number of each TAG<sup>75,76</sup>.

**Diatom photopigments.** For pigment analysis, 3 replicate aggregates from each treatment and sampling time point were individually transferred to 5 mL centrifugation tubes, snap-frozen in liquid nitrogen, and freeze-dried overnight. *Skeletonema marinoi* cultures were filtered onto 0.3 µm glass-fiber filters (GF75) that were snap-frozen in liquid nitrogen and freeze-dried overnight. Photopigments were extracted by adding 2.5 mL of HPLC-grade acetone: ethanol (1:1) to each sample and leaving it at -20 °C overnight. The extracted sample was centrifuged at

3700 g for 10 min and 1 mL of the supernatant was filtered through a 0.45 µm Versapor® membrane (Acrodisc®, Gelman Laboratory) into 2 mL glass vials with a septum cap. The extracted pigments were separated and analyzed on a Waters UPLC H-Class system equipped with an Acquity UPLC BEH C18 column (Waters, Milford, U.S.A.). Solvent gradients, column temperature, and flow rate were as described in ref. <sup>77</sup>. Photopigments were identified based on the retention time of the respective peak in the chromatogram and the associated absorption spectrum. The contents of the different photopigments identified in each aggregate or culture sample was calculated from the respective peak area and the calibration curve established on photopigment standards (DHI, Denmark).

**Microbial abundance.** At each sampling time point, the abundance of diatoms, bacteria, and viruses was determined in both the aggregate and the seawater surrounding the aggregate of three replicate exetainers for each treatment. After sample retrieval from the incubation tanks, the designated exetainers were placed upright for a few minutes to let the aggregate sink to the bottom. First, two 1 mL seawater samples were collected from the exetainer and transferred into two cryovials each containing 20 µL 0.2 µm-filtered glutaraldehyde; one cryovial was stored at 4 °C for light-microscopic diatom counts and one was stored at -80 °C for flow-cytometric analysis of bacterial and viral abundance. Second, the aggregate was thoroughly dispersed in the remaining seawater by vigorously pipetting the contents of the exetainer up and down for ~1 min. 1 mL of the resulting cell suspension was transferred into a cryovial containing 20 µL glutaraldehyde for light-microscopic diatom counts, while the remaining cell suspension was fixed with 60 µL glutaraldehyde and stored at -80 °C for flow-cytometric analysis. For quantification of bacteria and viruses on the particles, samples were sonicated at 40 kHz for 3 × 1 min with 30 s manual shaking between sonication, diluted 10-fold in Tris-EDTA buffer, stained with SYBR-Green I and measured on a BD FACS Canto™ II flow cytometer<sup>78</sup>.

Diatoms were counted in a Fuchs-Rosenthal counting chamber on a Zeiss Axio Lab.A1 light microscope at 400× magnification using phase contrast. Only cells with clearly discernible cell boundaries and chloroplasts were counted (= quantifiable cells), while strongly compromised cells were considered as degraded and thus not counted. For each sample, 10 grids each corresponding to a volume of 0.2 µL were counted and the result expressed per 1 mm<sup>3</sup> of aggregate volume. Diatoms were generally not detected in the seawater surrounding the aggregates, meaning that their abundance was <1 cell per 3.2 µL = <2 × 10<sup>3</sup> cells mL<sup>-1</sup>.

**Microbial community analysis.** Pressure effects on prokaryotic community composition of the aggregates were studied through 16 S rRNA gene amplicon sequencing. For this analysis, 3 replicate aggregates from each treatment and sampling time point were individually transferred to 5-mL, UV-sterilized centrifugation tubes, snap-frozen in liquid nitrogen, and stored at -80 °C until analysis. At t<sub>0</sub>, 7 replicate aggregates were sampled. DNA was extracted from the aggregates using the DNeasy PowerSoil Pro Kit (Qiagen No. 47016, Germany).

Amplification and barcoding of 16 S rRNA genes were done via two PCR rounds. The initial amplification was done using the universal 16 S rRNA gene primer pair 515F-Y (5'-GTGYCAGC MGCCGCGGTAA-3') with the adapter sequence (5'-TCGTCGG CAGCGTCAGATGTGTATAAGAGACAG-3') and 926 R (5'-CC GYCAATTYMTTTRAGTTT-3'), with the adapter sequence (5'-GTCTCGTGGGCTCGGAGATGTGTATAAGAGACAG-3'). The 25-µL PCR reactions contained 2 µL template DNA, 12.5 µL 2X KAPA HiFi Hotstart Readymix (KAPA Biosystems), 0.5 µL



bovine serum albumin (10 mg mL<sup>-1</sup>), 9 µL dH<sub>2</sub>O, and 0.5 µL of each primer (10 pmol µL<sup>-1</sup>). Cycling conditions were: 95 °C for 3 min, followed by 25 cycles of 95 °C for 30 s, 53 °C for 30 s and 72 °C for 30 s, with a final elongation at 72 °C for 10 min. In the second round of PCR, the PCR products were purified with the Agencourt AMPure XP PCR Purification system (Beckman Coulter) and indices added in another round of PCR using cycling conditions: 95 °C for 3 min, 12 cycles of 95 °C for 30 s, 55 °C for 30 s, and 72 °C for 30 s, with a final elongation at 72 °C for 5 min. Products were purified with AMPure XP beads and paired-end sequenced in 2 × 300 cycles on an Illumina MiSeq Desktop sequencer using the MiSeq v3 Reagent Kit according to standard protocols. Samples were sequenced in two separate MiSeq runs.

Trimming of adapter and PCR primers was done with cutadapt v0.11.1. The R package dada2 v. 1.18.0 was used for sequence filtering, denoising, paired-end merging and taxonomic classification. Samples from the two MiSeq runs were filtered and denoised separately to obtain an individual error model for each run with the DADA algorithm. After denoising, the two MiSeq runs were merged for detecting and removing chimeras. Finally, the amplicon sequence variants (ASVs) were taxonomically assigned using the Silva SSU reference database v. 138.1.

**Statistical analysis.** Significant effects of pressure on respiration activity, enzyme activities, DOC leakage, relative carbon loss, lipid and pigment contents, and microbial abundance at selected pressure levels were tested with two-tailed (except where otherwise noted) Student's *t*-tests. Significant changes in lipid contents and microbial abundance with increasing pressure were tested with two-tailed Student's *t*-tests of the slope of the respective variable versus pressure. Community analysis of the classified ASVs was done using the R packages phyloseq v1.34.0 and ampvis2 v2.6.5, and all plots were made with ggplot2 v3.3.3. We used vegan v2.5.7 for calculating analysis of similarity (ANOSIM) and permutational multivariate analysis of variance (PERMANOVA) tests.

**Reporting summary.** Further information on research design is available in the Nature Portfolio Reporting Summary linked to this article.

### Data availability

The source data for Figs. 2–5 and the Supplementary Figs. 1–6 have been deposited at PANGAEA (<https://doi.org/10.1594/PANGAEA.960357>)<sup>79</sup>. Sequencing data were deposited in the NCBI short-read archive (SRA) with the accession number PRJNA976707.

Received: 14 June 2023; Accepted: 4 October 2023;

Published online: 14 October 2023

### References

- Allredge, A. L. & Silver, M. W. Characteristics, dynamics and significance of marine snow. *Prog. Oceanogr.* **20**, 41–82 (1988).
- Simon, M., Grossart, H. P., Schweitzer, B. & Ploug, H. Microbial ecology of organic aggregates in aquatic ecosystems. *Aquat. Microb. Ecol.* **28**, 175–211 (2002).
- Turner, J. T. Zooplankton fecal pellets, marine snow, phytodetritus and the ocean's biological pump. *Prog. Oceanogr.* **130**, 205–248 (2015).
- Iversen, M. H. Carbon export in the ocean: A biologist's perspective. *Ann. Rev. Mar. Sci.* **15**, 357–381 (2023).
- Buesseler, K. O. et al. Revisiting carbon flux through the ocean's twilight zone. *Science* **316**, 567–570 (2007).
- Iversen, M. H., Nowald, N., Ploug, H., Jackson, G. A. & Fischer, G. High resolution profiles of vertical particulate organic matter export off Cape Blanc, Mauritania: Degradation processes and ballasting effects. *Deep-Sea Res.* **57**, 771–784 (2010).
- Jackson, G. A. & Checkley, D. M. Jr Particle size distributions in the upper 100 m water column and their implications for animal feeding in the plankton. *Deep-Sea Res.* **58**, 283–297 (2011).
- Belcher, A. et al. Depth-resolved particle-associated microbial respiration in the northeast Atlantic. *Biogeoscience* **13**, 4927–4943 (2016).
- Martin, J. H., Knauer, G. A., Karl, D. M. & Broenkow, W. W. VERTEX: carbon cycling in the northeast Pacific. *Deep-Sea Res.* **34**, 267–285 (1987).
- Silver, M. W. & Alldredge, A. L. Bathypelagic marine snow: deep-sea algal and detrital community. *J. Mar. Res.* **39**, 501–530 (1981).
- Iversen, M. H. & Ploug, H. Temperature effects on carbon-specific respiration rate and sinking velocity of diatom aggregates – potential implications for deep ocean export processes. *Biogeoscience* **10**, 4073–4085 (2013).
- Franco-Cisterna, B., Stief, P. & Glud, R. N. Temperature effects on carbon mineralization of sinking copepod carcasses. *Mar. Ecol. Prog. Ser.* **679**, 31–45 (2021).
- Tamburini, C. et al. Pressure effects on surface Mediterranean prokaryotes and biogenic silica dissolution during a diatom sinking experiment. *Aquat. Microb. Ecol.* **43**, 267–276 (2006).
- Stief, P., Elvert, M. & Glud, R. N. Respiration by 'marine snow' at high hydrostatic pressure: Insights from continuous oxygen measurements in a rotating pressure tank. *Limnol. Oceanogr.* **66**, 2797–2809 (2021).
- Tamburini, C. et al. Effects of hydrostatic pressure on microbial alteration of sinking fecal pellets. *Deep-Sea Res. Pt. II* **56**, 1533–1546 (2009).
- Amano, C. et al. Limited carbon cycling due to high-pressure effects on the deep-sea microbiome. *Nat. Geosci.* **15**, 1041–1047 (2022).
- Jaenicke, R. Biochemical processes under high hydrostatic pressure. *Naturwissenschaften* **70**, 332–341 (1983).
- Gross, M. & Jaenicke, R. Proteins under pressure. The influence of high hydrostatic pressure on structure, function and assembly of proteins and protein complexes. *Eur. J. Biochem.* **221**, 617–630 (1994).
- Bartlett, D. H. Pressure effects on in vivo microbial processes. *Biochim. Biophys. Acta* **1595**, 367–381 (2002).
- Oger, P. M. & Jebbar, M. The many ways of coping with pressure. *Res. Microbiol.* **161**, 799–809 (2010).
- Grossart, H.-P. & Gust, G. Hydrostatic pressure affects physiology and community structure of marine bacteria during settling to 4000 m: an experimental approach. *Mar. Ecol. Prog. Ser.* **390**, 97–104 (2009).
- Riou, V. et al. Biodegradation of *Emiliania huxleyi* aggregates by a natural Mediterranean prokaryotic community under increasing hydrostatic pressure. *Prog. Oceanogr.* **163**, 271–281 (2018).
- Thiele, S., Fuchs, B. M., Amann, R. & Iversen, M. H. Colonization in the photic zone and subsequent changes during sinking determine bacterial community composition in marine snow. *Appl. Environ. Microbiol.* **81**, 1463–1471 (2015).
- Oguri, K. et al. Hadal disturbance in the Japan Trench induced by the 2011 Tohoku-Oki earthquake. *Scientific Rep.* **3**, 1915 (2013).
- Mironov, A. N. et al. Echinoderms of the Kuril-Kamchatka Trench. *Prog. Oceanogr.* **179**, 102217 (2019).
- Fernández-Urruzola, I. et al. Plankton respiration in the Atacama Trench region: Implications for particulate organic carbon flux into the hadal realm. *Limnol. Oceanogr.* **66**, 3134–3148 (2021).
- Hutchins, D. A. & Bruland, K. W. Iron-limited diatom growth and Si:N uptake ratios in a coastal upwelling regime. *Nature* **393**, 561–564 (1998).
- Ren, J.-L. et al. Distribution of dissolved aluminium in the Southern Yellow Sea: Influences of a dust storm and the spring bloom. *Mar. Chem.* **125**, 69–81 (2011).
- Iversen, M. H. & Ploug, H. Ballast minerals and the sinking carbon flux in the ocean: carbon-specific respiration rates and sinking velocity of marine snow aggregates. *Biogeoscience* **7**, 2613–2624 (2010).
- Elling, F. J. et al. Respiratory quinones in Archaea: phylogenetic distribution and application as biomarkers in the marine environment. *Environ. Microbiol.* **18**, 692–707 (2016).
- Norici, A., Bazzoni, A. M., Pugnetti, A., Raven, J. A. & Giordano, M. Impact of irradiance on the C allocation in the coastal marine diatom *Skeletonema marinoi* Sarno and Zingone. *Plant Cell Environ.* **34**, 1666–1677 (2011).
- Fukuda, R., Ogawa, H., Nagata, T. & Koike, I. Direct determination of carbon and nitrogen contents of natural bacterial assemblages in marine environments. *Appl. Environ. Microbiol.* **64**, 3352–3358 (1998).
- Steward, G. F., Fandino, L. B., Hollibaugh, J. T., Whitledge, T. E. & Azam, F. Microbial biomass and viral infections of heterotrophic prokaryotes in the sub-surface layer of the central Arctic Ocean. *Deep-Sea Res.* **54**, 1744–1757 (2007).
- Eisenmenger, M. J. & Reyes-De-Corcuera, J. I. High pressure enhancement of enzymes: A review. *Enzyme Microb. Technol.* **45**, 331–347 (2009).
- Lampitt, R. S. et al. Ocean fertilization: a potential means of geoengineering? *Phil. Trans. R. Soc. A* **366**, 3919–3945 (2008).
- Passow, U. & Carlson, C. A. The biological carbon pump in a high CO<sub>2</sub> world. *Mar. Ecol. Prog. Ser.* **470**, 249–271 (2012).

37. Ducklow, H. W., Steinberg, D. K. & Buesseler, K. O. Upper ocean carbon export and the biological pump. *Oceanogr.* **14**, 50–58 (2001).
38. Burdige, D. J. Preservation of organic matter in marine sediments: Controls, mechanisms, and an imbalance in sediment organic carbon budgets? *Chem. Rev.* **107**, 467–485 (2007).
39. Dittmar, T. et al. Enigmatic persistence of dissolved organic matter in the ocean. *Nat. Rev. Earth Environ.* **2**, 570–583 (2021).
40. Becker, S. et al. Laminarin is a major molecule in the marine carbon cycle. *Proc. Natl. Acad. Sci.* **117**, 6599–6607 (2020).
41. Vidal-Melgosa, S. et al. Diatom fucan polysaccharide precipitates carbon during algal blooms. *Nat. Comm.* **12**, 1150 (2021).
42. Huang, G. et al. Secretion of sulfated fucans by diatoms may contribute to marine aggregate formation. *Limnol. Oceanogr.* **66**, 3768–3782 (2021).
43. Balcombe, J. P., Simon, M., Giebel, H. A. & Arnosti, C. A sea change in microbial enzymes: Heterogeneous latitudinal and depth-related gradients in bulk water and particle-associated enzymatic activities from 30°S to 59°N in the Pacific Ocean. *Limnol. Oceanogr.* **66**, 3489–3507 (2021).
44. Buck-Wiese, H. et al. Fucoid brown algae inject fucoic acid into the ocean. *Proc. Natl. Acad. Sci. U.S.A.* **120**, e2210561119 (2023).
45. Stocker, R., J. R. Seymour, A. Samadani, D. E. Hunt, and M. F. Polz. Rapid chemotactic response enables marine bacteria to exploit ephemeral microscale nutrient patches. *Proc. Natl. Acad. Sci. U.S.A.* **105**: 4209–4214 (2008).
46. Bendtsen, J., Lundsgaard, C., Middelboe, M. & Archer, D. Influence of bacterial uptake on deep-ocean dissolved organic carbon. *Global Biogeochem. Cycles* **16**, 1127 (2002).
47. Wakeham, S. G., Lee, C., Hedges, J. L., Hernes, P. J. & Peterson, M. J. Molecular indicators of diagenetic status in marine organic matter. *Geochim. Cosmochim. Acta.* **61**, 5363–5369 (1997).
48. Zhao, L., Dai, J. & Wu, Q. Autophagy-like processes are involved in lipid droplet degradation in *Auxenochlorella protothecoides* during the heterotrophy-autotrophy transition. *Front. Plant Sci.* **5**, 400 (2014).
49. Joli, N. et al. Hypometabolism to survive the long polar night in the diatom *Fragilariopsis cylindrus*. *bioRxiv*. <https://doi.org/10.1101/2023.01.14.524047> (2023).
50. Pelusi, A. et al. Gene expression during the formation of resting spores induced by nitrogen starvation in the marine diatom *Chaetoceros socialis*. *BMC Genomics* **24**, 106 (2023).
51. Kuwata, A., Hama, T. & Takahashi, M. Ecophysiological characterization of two life forms, resting spores and resting cells, of a marine planktonic diatom, *Chaetoceros pseudocurvisetus*, formed under nutrient depletion. *Mar. Ecol. Prog. Ser.* **102**, 245–255 (1993).
52. Kuwata, A. & Takahashi, M. Survival and recovery of resting spores and resting cells of the marine planktonic diatom *Chaetoceros pseudocurvisetus* under fluctuating nitrate conditions. *Mar. Biol.* **134**, 471–478 (1999).
53. Pelusi, A., Santelia, M. E., Benvenuto, G., Godhe, A. & Montresor, M. The diatom *Chaetoceros socialis*: spore formation and preservation. *Europ. J. Phycol.* **55**, 1–10 (2020).
54. Itakura, S., Imai, I. & Itoh, K. “Seed bank” of coastal planktonic diatoms in bottom sediments of Hiroshima Bay, Seto Inland Sea, Japan. *Mar. Biol.* **128**, 497–508 (1997).
55. Salter, I. et al. Diatom resting spore ecology drives enhanced carbon export from a naturally iron-fertilized bloom in the Southern Ocean. *Global Biogeochem. Cycles* **26**, GB1014 (2012).
56. Rynearson, T. A., Richardson, K., Lampitt, R. S., Sieracki, M. E. & Poulton, A. J. Major contribution of diatom resting spores to vertical flux in the sub-polar North Atlantic. *Deep-Sea Res.* **82**, 60–71 (2013).
57. Rembauville, M., Manno, C., Tarling, G. A., Blain, S. & Salter, I. Strong contribution of diatom resting spores to deep-sea carbon transfer in naturally iron-fertilized waters downstream of South Georgia. *Deep-Sea Res.* **115**, 22–35 (2016).
58. Smith, C. R. et al. Phytodetritus at the abyssal seafloor across 10 degrees of latitude in the central equatorial Pacific. *Deep-Sea Res.* **43**, 1309–1338 (1996).
59. Agusti, S. et al. Ubiquitous healthy diatoms in the deep sea confirm deep carbon injection by the biological pump. *Nat. Comm.* **6**, 7608 (2015).
60. Bochdansky, A. B., Clouse, M. A. & Herndl, G. J. Eukaryotic microbes, principally fungi and labyrinthulomycetes, dominate biomass on bathypelagic marine snow. *ISME J.* **11**, 362–373 (2017).
61. Romero, O. E. et al. Flux variability of phyto- and zooplankton communities in the Mauritanian coastal upwelling between 2003 and 2008. *Biogeosciences* **17**, 187–214 (2020).
62. Poff, K. E., Leua, A. O., Eppley, J. M., Karl, D. M. & DeLong, E. F. Microbial dynamics of elevated carbon flux in the open ocean’s abyss. *Proc. Natl. Acad. Sci.* **118**, e2018269118 (2021).
63. Glud, R. N. et al. High rates of microbial carbon turnover in sediments in the deepest oceanic trench on Earth. *Nat. Geosci.* **6**, 284–288 (2013).
64. Glud, R. N. et al. Hadal trenches are dynamic hotspots for early diagenesis in the deep sea. *Commun. Earth Env.* **2**, 21 (2021).
65. Wenzhöfer, F. K. et al. Benthic carbon mineralization in hadal trenches: Assessment by in situ O<sub>2</sub> microprofile measurements. *Deep Sea Res.* **116**, 276–286 (2016).
66. Schaubberger, C. et al. Microbial community structure in hadal sediments: high similarity along trench axes and strong changes along redox gradients. *ISME J.* **15**, 3455–3467 (2021).
67. Stief, P., Kamp, A., Thamdrup, B. & Glud, R. N. Anaerobic nitrogen turnover by sinking diatom aggregates at varying ambient oxygen levels. *Front. Microbiol.* **7**, 98 (2016).
68. Guillard, R. R. L. & Hargraves, P. E. *Stichochrysis immobilis* is a diatom, not a chrysophyte. *Phycologia* **32**, 234–236 (1993).
69. Fine, R. A. & Millero, F. J. Compressibility of water as a function of temperature and pressure. *J. Chem. Phys.* **59**, 5529–5536 (1973).
70. Glud, R. N. et al. Adaptation, test and in situ measurements with O<sub>2</sub> microopt(r)odes on benthic landers. *Deep Sea Res.* **26**, 171–183 (1999).
71. Stief, P. and others. Intracellular nitrate storage by diatoms can be an important nitrogen pool in freshwater and marine ecosystems. *Commun. Earth Environ.* **3**, 154 (2022).
72. Popendorf, K. J., Fredricks, H. F. & Van Mooy, B. A. S. Molecular ion-independent quantification of polar glycerolipid classes in marine plankton using triple quadrupole MS. *Lipids* **48**, 185–195 (2013).
73. Becker, K. W., Lipp, J. S., Zhu, C., Liu, X. L. & Hinrichs, K. U. An improved method for the analysis of archaeal and bacterial ether core lipids. *Org. Geochem.* **61**, 34–44 (2013).
74. Wörmer, L., Cires, S., Velazquez, D., Quesada, A. & Hinrichs, K. U. Cyanobacterial heterocyst glycolipids in cultures and environmental samples: Diversity and biomarker potential. *Limnol. Oceanogr.* **57**, 1775–1788 (2012).
75. Holcapek, M., Lisa, M., Jandera, P. & Kabatova, N. Quantitation of triacylglycerols in plant oils using HPLC with APCI-MS, evaporative light-scattering, and UV detection. *J. Sep. Sci.* **28**, 1315–1333 (2005).
76. Becker, K. W. and others. Daily changes in phytoplankton lipidomes reveal mechanisms of energy storage in the open ocean. *Nat. Comm.* **9**, 5179 (2018).
77. Meier, D. V. et al. Limitation of microbial processes at saturation-level salinities in a microbial mat covering a coastal salt flat. *Appl. Environ. Microbiol.* **87**, e00698–21 (2021).
78. Schaubberger, C. et al. Spatial variability of prokaryotic and viral abundances in the Kermadec and Atacama Trench regions. *Limnol. Oceanogr.* **66**, 2095–2109 (2021).
79. Stief, P. and others. 2023. Effects of increasing hydrostatic pressure on sinking diatom aggregates. *PANGAEA*, <https://doi.org/10.1594/PANGAEA.960357>.

## Acknowledgements

We would like to thank Anni Glud, Birthe Christensen, Morten Alitouche Kieler, Feiyang Gu, Erik Laursen, Martina Alisch, Gaby Eickert-Groetzschel, Clemens Röttgen, Stephanie Caddell, Sherif Ghobrial, Leah Brinch Iversen, and Hans Frederik Hansen for technical assistance. We also thank Carol Arnosti for kindly providing the FLA-labelled polysaccharide substrates for the enzyme activity measurements. This study was financially supported by the Danish National Research Foundation through the Danish Center for Hadal Research (HADAL, Grant No. DNRF145) and the European Union’s Horizon 2020 Research and Innovation Program (HADES-ERC, Grant agreement No. 669947). Laboratory work by ME was supported by Deutsche Forschungsgemeinschaft through the Cluster of Excellence EXC 2077 “The Ocean Floor - Earth’s Uncharted Interface” (Project No. 390741601).

## Author contributions

P.S., R.N.G., C.S. and J.P.B. designed the study. P.S., C.S., J.P.B. and B.F.C. carried out the pressure-tank experiments. P.S., C.S., K.B., M.E., J.P.B. and MM analyzed samples and interpreted data. P.S. conceived and wrote the manuscript with inputs from all co-authors.

## Competing interests

The authors declare no competing interests.

## Additional information

**Supplementary information** The online version contains supplementary material available at <https://doi.org/10.1038/s43247-023-01045-4>.

**Correspondence** and requests for materials should be addressed to Peter Stief.

**Peer review information** *Communications Earth & Environment* thanks Barbara Bayer and the other, anonymous, reviewer(s) for their contribution to the peer review of this work. Primary Handling Editors: Erin Bertrand, Clare Davis. A peer review file is available.

**Reprints and permission information** is available at <http://www.nature.com/reprints>

**Publisher’s note** Springer Nature remains neutral with regard to jurisdictional claims in published maps and institutional affiliations.





**Open Access** This article is licensed under a Creative Commons Attribution 4.0 International License, which permits use, sharing, adaptation, distribution and reproduction in any medium or format, as long as you give appropriate credit to the original author(s) and the source, provide a link to the Creative Commons licence, and indicate if changes were made. The images or other third party material in this article are included in the article's Creative Commons licence, unless indicated otherwise in a credit line to the material. If material is not included in the article's Creative Commons licence and your intended use is not permitted by statutory regulation or exceeds the permitted use, you will need to obtain permission directly from the copyright holder. To view a copy of this licence, visit <http://creativecommons.org/licenses/by/4.0/>.

© The Author(s) 2023